SYNTHESIS AND ELECTRICAL CHARACTERIZATION OF ZINC STANNATE (ZTO) PREPARED BY HYDROTHERMAL METHOD

*D. RUIZ-LEÓN[a], *R. E. AVILA[b], C. J. VENEGAS[a]

[a)] Chemistry Materials Department, Universidad de Santiago de Chile, Av. Libertador Bernardo O'Higgins nº 3363, Santiago, Chile.
[b)] Personal Dosimetry Section, Chilean Nuclear Energy Commission, Santiago, Chile

ABSTRACT

Zinc Stannate was prepared at 200 °C by hydrothermal method. The X-Ray diffraction data indicate the obtained compound crystallized in the Fd3m space group characteristic of a cubic spinel structure. SEM-EDX and backscattered electrons show and confirm the purity and homogeneity of the final sample. The ZTO pressed pellet, sintered at 825 ºC, for 1 h, reveals a single, slightly flattened, impedance semicircle and homogeneous electrical microstructure.

Keywords: Electroceramic, Conducting Oxide, Impedance Spectroscopy, DRX

INTRODUCTION

ZnO-based materials have a wide spectrum of applications, both as bulk polycrystalline ceramics and films. The interest on these materials has been renewed because of their potential for obtaining transparent conductors, magnetic semiconductors, and improved gas sensing elements[1]. For this purpose, much research is being focused on the control of the ZnO electrical response, in particular by doping with different ions. Undoped ZnO crystallizes in the wurtzite structure and due to its native defects exhibits n-type conduction. However, proper p-type conductivity can also be rendered by proper doping using appropriate ions. Reported results on the role played by several dopants on the material microstructure and electrical response are often contradictory. Actually Basic issues such as, for instance, the solid solubility limit of certain cations into the ZnO lattice are still unclear[2-4]. Variability in the data scattering found in literature is also favoured by the impact on the material reliability of the different processing used either for bulk materials or films. Recently, the electrical behavior of Sn-doped ZnO thin films grown by pulsed laser deposition (PLD) has been reported[5]. Doping ZnO films with a nominal value of 0.1 mol% SnO_2 show a lower resistivity than undoped ZnO ones, this is in agreement with the incorporation of Sn^{4+} at Zn^{2+} lattice sites. However if the SnO_2 concentration is increased further, the electrical resistivity also increases and the cubic Zn_2SnO_4 spinel-type phase appears as a secondary phase. The Zn_2SnO_4 (ZTO) spinel phase has been synthesized as nanosized particles with different shapes[6-9], however few little data has been found regarding the electrical behaviour properties of the pure phase. Reported data on ZTO thin films[10] show that their electrical resistivity is on the order of 10^{-2} Ωcm as is also reported for ZnO films.

ZTO nanosized particles with very fine grains show electrical resistivity values[11] on the order of 10^7 Ωcm, which is nine orders of magnitude higher than that reported for ZTO thin films. Nevertheless, the porosity of these samples (approximately 40% in the sintered sample) does not facilitate direct comparison to thin films or denser ceramic samples.

In addition, pay attention to the commercial terms that conventionally require this type of new materials it is not enough, since at first stage we must take into account the synthetic conditions and how these conditions can modify the physical properties. A very good example of this is given by the synthesis of $BaTiO_3$ particles, a well-known dielectric material that is largely used in the electroceramics industry for the production of cellular phones. This type of phase is produced via solid-state reactions[12], sol-gel methods[13-14] and hydrothermal synthesis[15-17]. For the solid state reaction, $BaTiO_3$ particles were synthesized through the reaction of TiO_2 and $BaCO_3$ at 1500 ºC for 24 hrs. This process is simple but useless because the obtained particles are too large (several micrometers) and logically grind them, may introduce impurities. Using sol-gel method low temperatures, it is possible to obtain particles of high purity and particle size ranging from 10 nm to 100 nm. However, the reagents are expensive and the synthetic process is complex. Conversely, hydrothermal synthesis has proven to be one of the best methods to produce particles of metal oxides. $BaTiO_3$ particles obtained through this method have been synthesized from titanium and barium salts at temperatures between 90 and 200 ºC. This method has many advantages. Among them can be mentioned the highly crystalline materials obtained, low reaction temperatures, and simpler reaction procedure once the ideal experimental conditions are known.

The hydrothermal synthesis is achieved from chemical reactions performed in a sealed container held at temperatures above room temperature and auto generated pressures. The hydrothermal synthesis enables reactions to occur at extreme conditions; the physicochemical properties of the solutions are altered as a result of the highly-pressurized system. The mechanism of the hydrothermal reactions can be described by a liquid nucleation model[18] which is distinct from the solid state synthesis. Hydrothermal synthesis is described by a reaction resulting from the diffusion of atoms and ions in the interphase between the reactants. This method has been successfully utilized in the synthesis of solid phases such as microporous crystals, super-ionic conductors, chemical sensors, conducting electronic solids, and magnetic materials[19-23]. Moreover, this synthesis can be used for obtaining condensed phases including nanometric particles, gels, films, and materials featuring unusual packing.

In this context, zinc stannate, Zn_2SnO_4, a ternary oxide spinel, is an interesting semiconducting material in the family of transparent conducting oxides. Zn_2SnO_4 and is well known to display a high sensitivity to various gases, with high intrinsic electrical resistivity, making it suitable for a wide range of applications, such as humidity sensors, transparent conducting electrodes and negative electrode for Li-ion batteries[24]

In recent years, ZTO has been successfully prepared by various methods (thermal evaporation, sol-gel synthesis, and mechanochemical activation followed by solid-state reactions)[25-26]. However, the electrical features of ZTO prepared by hydrothermal synthesis have received little attention[27]. In this work the hydrothermal synthesis of pure ZTO is discussed, and its bulk material electrical properties are characterized by impedance spectroscopy.

EXPERIMENTAL

Zinc chloride ($ZnCl_2$) and tin tetrachloride ($SnCl_4 \cdot 5H_2O$) were used as the zinc and tin sources, respectively, for the hydrothermal synthesis of Zn_2SnO_4. The two sources were dissolved in distilled water to form two transparent solutions. The tin tetrachloride solution was slowly added to the zinc chloride solution. A molar ratio Zn:Sn of 2:1 was maintained throughout this work. As a mineralizer, sodium carbonate (Na_2CO_3) solution was added drop-wise to the mixture under magnetic stirring. Various Na_2CO_3 concentrations with Zn:Sn:Na_2CO_3 ratios of 2:1:2, 2:1:4 and 2:1:6 were made in order to investigate the effects of concentration of the mineralizer. After magnetic stirring for 15 min, the slurry was transferred into a 23 mL Teflon-lined stainless steel autoclave. The mixture was subjected to hydrothermal conditions in the temperature range of 120–230 °C for up to 30 h. After the reaction, the autoclave was naturally cooled to room temperature. The resulting precipitates were centrifuged at 3000 rpm, washed three times with distilled water and twice with ethanol successively, and dried at 60 °C in an oven for 8 h before further characterization.

The X-ray diffraction (XRD) data were collected at room temperature on a Siemens D5000 powder diffractometer, with CuK_a radiation in the range $5º < 2\theta < 80º$, with counting time of 1 s over the 0.02 °(2θ) steps.

For electrical characterization, the opposite flat surfaces of the samples were sputtered with platinum and sandwiched between the platinum electrodes of the sample holder during measurements. The sample holder consisted of a quartz tube, fitted with a K-type thermocouple, ~7 mm from the sample, within a 200 - 500 standard cubic centimeter per second dry air flow. An external

e-mail address: domingo.ruiz@usach.cl

cylindrical oven provided for temperature control in the room temperature to 1100 K range. The linearity of the Pt-ZTO contacts was established by *dc* I-V measurements using a Keithley 237 electrometer. Then, the temperature dependence of the conductivity was studied from room temperature to 1000 K up and down ramps. To avoid the possibility of polarizing the pellet-electrode interfaces over the time-consuming temperature measurement studies, the current was measured with a square wave. 10 s were allowed during both the positive and negative pulses, during which the current was measured continuously, at ~70 ms intervals, and the average over the last 3 measurements was recorded. Next, the difference of those averages, from the negative pulse to the positive one was registered, and divided by twice the pulse magnitude to obtain the conductivity of the pellet.

Impedance-frequency measurements were carried out with a Solartron SI-1260 impedance gain-phase analyzer in the frequency range of 0.1 Hz to 10 MHz with an *ac* signal level of 1 V, to probe the charge transport mechanism that may not be accessible through the dc I-V measurements. The ZTO pressed pellet was sintered at 825 ºC, for 1 h.

The surface morphology and composition were inspected by SEM-EDX and backscattered electrons microscopy.

RESULTS AND DISCUSSION

Comparison of the XRD powder pattern (Figure 1) with the database reference confirms the purity and the homogeneity of the sample. Figure 2 depicts the diffraction pattern calculated from the analysis of a sample of polycrystalline powder using the Rietveld method. The values of experimental error are R_{wp} = 8.5, R_{exp} = 7.2 and χ^2 = 3.1. The analysis of the structure shows that the synthesized phase corresponds to an inverse spinel which crystallized in a cubic system with space group F d 3 m and a lattice constant value of 8.657 Å. The atomic arrangement for this type of spinel is $Zn_{tet}(Zn, Sn)_{oct}O_4$.

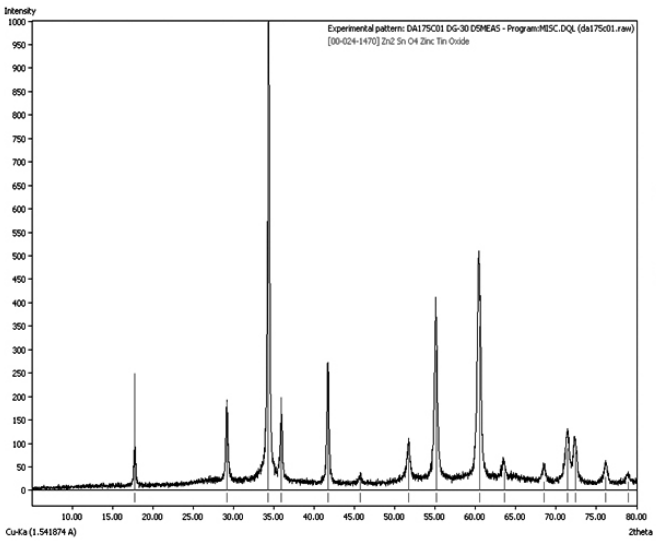

Fig. 1: XRD pattern of Zn_2SnO_4 compared with database.

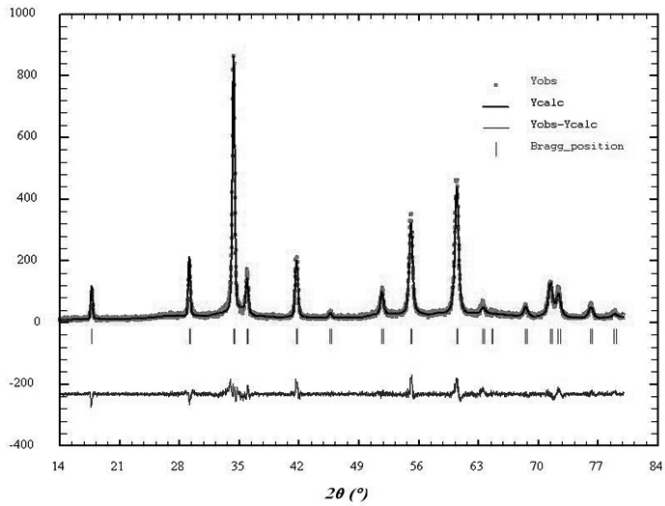

Fig. 2: XRD pattern of Zn_2SnO_4, sintered at 825 °C for 1 h.

SEM microscopy image in Figure 3, shows a ZTO nanosized material, crystallized in a cubic shape with an average size of 80 nm.

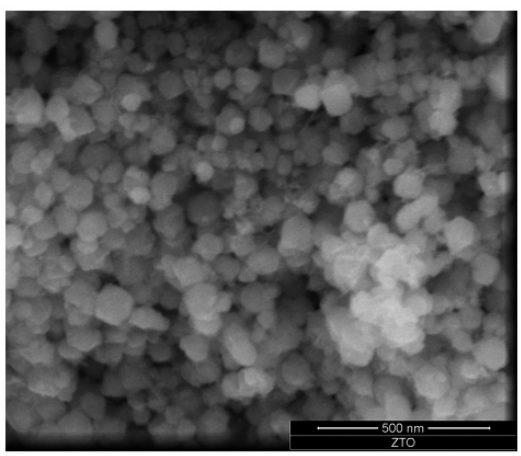

Fig. 3: SEM image of nanosized Zn_2SnO_4

Under SEM-EDX microscopy, the purity and homogeneity of the intended oxide is confirmed, as shown in Figure 4.

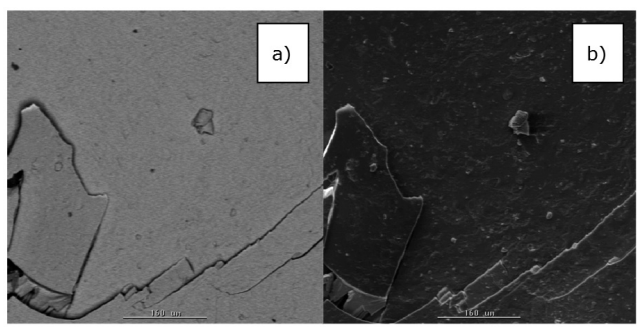

Fig. 4: a) Zn_2SnO_4 backscattered electron image.
b) Secondary electrons image for the microstructure of Zn_2SnO_4 pebble, sintered at 825 °C for 1 h.

The *dc I-V* curves obtained were linear, supporting the Ohmic character of the contacts. A high sensitivity to humidity is revealed both by *ac* impedance and by *dc* current-time measurements, grossly demonstrated by three orders of magnitude increase in the impedance from dry air to 40% relative humidity as can be seen in Figure 5.

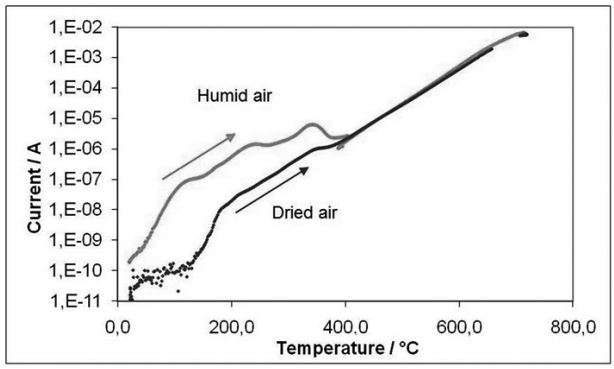

Fig. 5: Current vs temperature plot between humid and dried air

During an upwards temperature ramp, after over a week since the last heating cycle, the conductivity increases, displaying at least two deviations from the classical Arrhenius behavior. These deviations are shown in Figure 6a, near 530 and 600 K, respectively, as drops from the projection of the conductivity increase in the temperature range immediately precedes the deviation. These deviations in the conductivity coincide with deviations in the capacitance, as seen in Figure 6b. Both views of the electrical transport behavior suggest some structural transitions in the material.

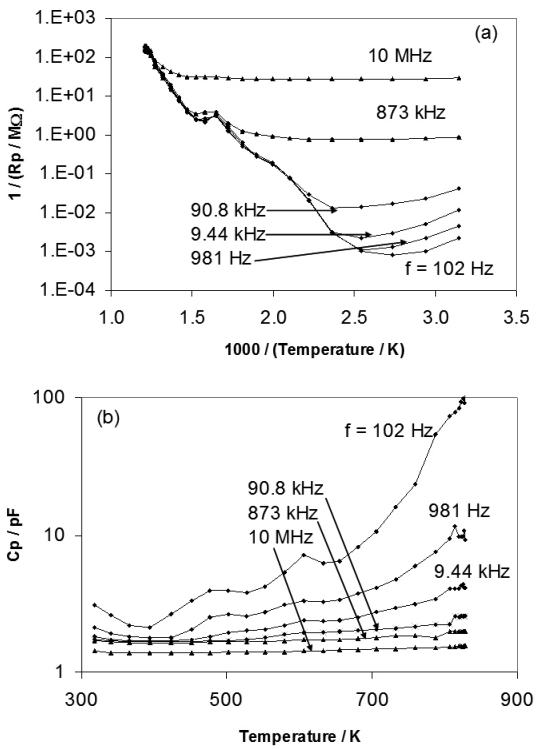

Fig. 6: Parallel conductivity - capacitance representation:

(a) Arrhenius plot of the parallel conductivity.

(b) The parallel capacitance.

However, during the ensuing downwards temperature ramp, only slights deviations from the Arrhenius behavior is observed, as shown in Fig. 6, registered by the pulsed *dc* scan method, from 993 to 339 K (720 to 66 °C), at 4 K/min. The resulting Arrhenius plot suggests that more than one hindrance to the carrier transport is active over the temperature range, with an overall activation energy of ~0.92 eV.

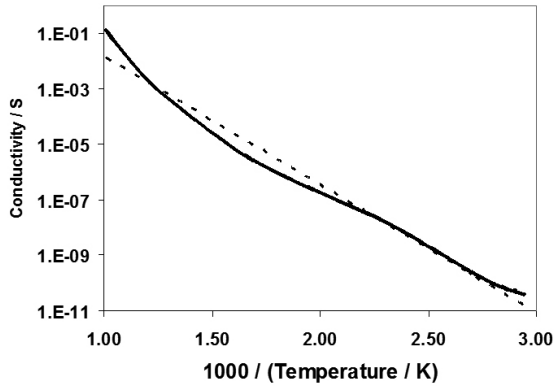

Fig. 7: Temperature activation of the conductivity.

From another temperature cycle, the frequency curves as a function of impedance were measured during the downward temperature ramp (Figure 8).

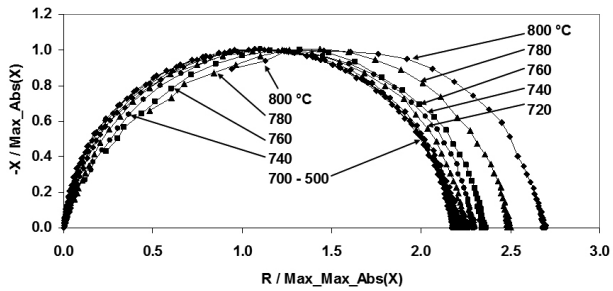

Fig. 8: Nyquist plots scaled by the maximum value of (-X)

In order to characterize the microstructures and properties of electroceramics, different techniques are required that can probe or distinguish between the different regions of a ceramic[28]. For instance, from a microscopic examination of ceramic texture, it is not usually possible to say whether the electrical properties of grain boundaries are likely to be similar to or significantly different from those of the individual grains[29]. From an impedance/modulus spectroscopic plot in the former case, grains and grain boundaries can be distinguishable electrically. The value of presenting data as both M" and Z" spectroscopic plots is that they give different weightings to the data and therefore, highlight different features of the sample.

The impedance – frequency curve presented in Figure 9, reveals single, slightly flattened Impedance semicircles at different temperatures. The capacitance value was fitted from a resistance and a constant phase element (CPE). The calculated value for the resistance is 3,2E7 Ωcm, which is consistent with a previous reported result[11]. The obtained capacitance value is 2,94E-12 corresponding to a single element associated to the grain microstructure.

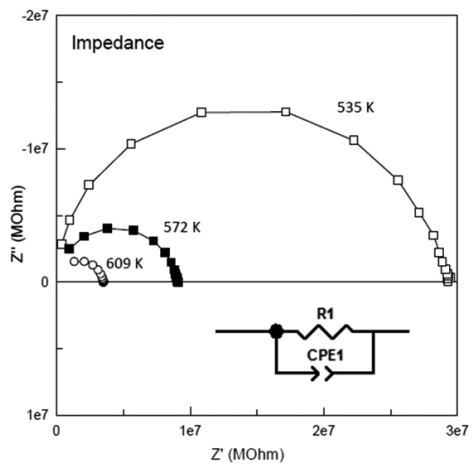

Fig. 9: Impedance plot for Zn_2SnO_4

In Figure 10 the M" and Z" spectroscopic plots shows that the most resistive element is overlapped with the smallest capacitance element suggesting a homogeneous grain electrical behavior for the ZTO nanosized phase. This is in agreement with the impedance plot depicting a single bulk element[30].

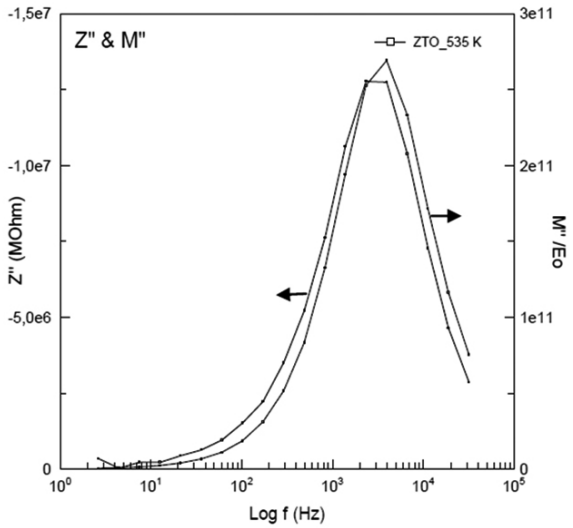

Fig. 10: M" and Z" spectroscopic plots for Zn_2SnO_4

CONCLUSIONS

Zn_2SnO_4 can be synthesized as a chemically pure nanosized sample by using the hydrothermal method. The impedance analysis for the electrical properties in addition with the spectroscopic plots, reveals a single, slightly flattened; Impedance semicircle that can be fitted with a resistance and constant phase element (CPE) in parallel showing a ceramic material with an electrical homogenous behavior dominated by a bulk grain microstructure.

ACKNOWLEDGMENT

The support of FONDECYT, under grant 11085067 is greatly appreciated and LIA MIF 836

REFERENCES

1. M. Bouderbala, S. Hamzaoui, B. Amrani, A.H. Reshak, M. Adnane, T. Sahraoui, M. Zerdali, Physica B, **403**, 3326, (2008)
2. J. Yang, J. Lee, K. Im, S. Lim, Physica E, **42**, 51, (2009)
3. Ü. Özgür, Ya.I. Alivov, C. Liu, A. Teke, M.A. Reshchikov, S. Doğan, V. Avrutin, S.-J. Cho, H. Morkoç, J. Appl. Phys. **98**, 041301, (2005)
4. A. Bedia, F.Z. Bedia, M. Aillerie, N. Maloufi, S. Ould Saad Hamady, O. Perroud, B. Benyoucef, Opt. Mater., **36**, 1123, (2014)
5. M.S. Al-Assiri, M.M. Mostafa, M.A. Ali, M.M. El-Desoky, Superlattices Microstruct., **75**, 127, (2014)
6. A. Annamalai, D. Carvalho, K.C. Wilson, M.J. Lee, Mater Charact., **61**, 873, (2010)
7. H.F. Lin, S.C. Liao, S.W. Hung, C.T. Hu, Mater Chem Phys, **117**, 9, (2009)
8. X. Ji, X. Huang, J. Liu, J. Jiang, X. Li, R. Ding, Y. Hu, F. Wu, Q. Li, J Alloys Compd., **503**, L21, (2010)
9. R. Jose, V. Thavasi, S. Ramakrishna, J. Am. Ceram. Soc, **92**, 289, (2009)
10. J. H Yu, G. M Choi, Sens. Actuators B: Chem., **72**, 141, (2001)
11. Y. Iglesias, M. Peiteado, J. de Frutos, A.C. Caballero., J. Euro. Ceram. Soc, **27**, 3931, (2007)
12. H. -I. Hsiang, Y.-L Chang, J.-S Fang, F.-S. Yen, J. Alloys Compd, 509, 7632, (2011)
13. Y. Xie, J. Am. Ceram. Soc., **82**, 768, (1999)
14. R. Ashiri, A. Nemati, M. Sasani Ghamsari., Ceram. Inter., **40**, 8613, (2014)
15. W. Wang, L. Cao, W. Liu, G. Su, W. Zhang, Ceram. Inter., **39**, 7127, (2013)
16. X. Yang, Z. Ren, G. Xu, C.Chao, S. Jiang, S. Deng, G. Shen, X. Wei, G. Han, Ceram. Inter., **40**, 9663, (2014)
17. Y. Hotta, C. Duran, K. Sato, T. Nagaoka, K. Watari, J. Euro. Ceram. Soc., **28**, 599, (2008)
18. S.-W. Chen, J.-M. Wu, Acta Materialia, **59**, 841, (2011)
19. J. Kim, J.-D. Jeon, S.-Y. Kwak, Microp. Mesop. Mater., **168**, 148, (2013)
20. K. Byrappa, S. Srikantaswamy, G.S. Gopalakrishna, A.B. Kulkarni, J.Shashidhara Prasad, Solid State Ionics, **24**, 1, (1987)
21. H. Wang, Y. Qu, H. Chen, Z. Lin, K. Dai, Sens. Actuators B: Chem., **201**,153, (2014)
22. S.-H. Hsu, S.-F. Hung, S.-H. Chien, J. Power Sources, **233**, 236, (2013)
23. H. Niu, J. Chen, Q. Niu, Y. Gao, J. Song, C. Mao, S. Zhang, Q. Chen, J. Cryst. Growth, **329**,82, (2011)
24. K. Wang, Y. Huang, Y. Shen, L. Xue, H. Huang, H. Wu, Y. Wang, Ceram. Inter., **40**, 15183, (2014)
25. E. L. Foletto, J. M. Simões, M. A. Mazutti, S. L. Jahn, E. I. Muller, L. S.-Fagundes Pereira, E. M. de Moraes Flores, Ceram. Inter., **39**, 4569, (2013)
26. T. Lana-Villarreal, G. Boschloo, A. Hagfeldt , J. Phys. Chem. C, **111**, 5549, (2007)
27. X. Hou, Q. Cheng, Y. Bai, W.F. Zhang, Solid State Ionics, **181**, 631, (2010)
28. P. R. Bueno, J. A. Varela, E. Longo, J. Euro. Ceram. Soc., **27**, 4313, (2007)
29. A. R. West, C. Sinclair, N. Hirose, J. Electroceram., 1, 65, (1997)
30. J. T. S. Irvine, D. C Sinclair, A. R. West, Adv. Mater., **2**, 132, (1990)